Sensors & Transducers, Vol. 165, Issue 2, February 2014, pp. 142-149

www.sensorsportal.com

Sensors & Transducers

http://www.sensorsportal.com

Performance Investigation of the Impact Mechanisms of Turbulence Image Mathematical Properties

*** Zhongwei Liang, Bangyan Ye**
School of Mechanical and Automobile Engineering, South China University of Technology, Guangzhou, 510640, China
* Tel.: 13416240167, fax: 0862039366923
* E-mail: lzwstalin@126.com

Received: 20 November 2013 /Accepted: 28 January 2014 /Published: 28 February 2014

Abstract: In this research, fuzzy gray degrees were established to quantitatively evaluate the impact mechanisms in the image properties of turbulence motion locus. Through selecting different impact mechanisms during image acquirement and establishing factor-parameters array, the mathematical model of fuzzy gray evaluating system can therefore be structured. After calculating those fuzzy gray relational degrees between those factor-parameters and image properties, the external impact on image properties can be quantized systematically. By repeatedly experiments their impact disciplines are determined, this paper also provides technical references and new research ideas for following turbulence monitoring in practice as well. *Copyright © 2014 IFSA Publishing, S. L.*

Keywords: Turbulence, Image properties, Impact mechanisms, Performance Investigation.

1. Introduction

Analysis in the influential mechanism between turbulence imaging and experimental conditions in confined space exerts a considerable impact on turbulence simulation and becomes a difficult problem in fluid theory research as well. Though turbulence image reflects the acceptability of turbulence simulation and computation in accuracy and veracity, the mutual relationship and performance comparison of them still remain unstudied and undeveloped in these years.

It can be easily seen that turbulence image characteristic in a confined space plays a pivotal role in following fluid field monitoring.

Nowadays many technical developments have been achieved, such as Thrasyvoulos Panidis *et al.* [1] identified the impact of the dispersed phase on the initially isotropic turbulence field, and discussed the physical processes responsible for the observed image changes as well; Serhat Kucukali *et al.* [2], Satya P. Ojha *et al.* [3] and John Villasenor *et al.* [4] have studied turbulence images in different experimental conditions and scientific methods, thus their respective impact mechanisms were discussed in detail, with relative efforts were also be described in [5-8]; on the other hand, G. H. Rhee [9] and A. S. Pereira *et al.* [10] have conducted the experimental fluid imaging respectively; Bruce L. Rhoads *et al.* [11] have presented several impact mechanisms of low-stage flows yet, all these efforts contribute to the turbulence influential factor researches. It can be also found that Wang Zhen-B [12] and E. A. Luke *et al.* [13] have conducted some imaging experiments concerning with turbulence properties and its impact mechanism as well. After searching those theoretical literatures and reviewing various previous efforts it can be concluded that most

Article number P_1891

turbulence experiments focused on their flow properties or spatial simulations, nevertheless fluid properties and their detailed computation processes still remain unstudied yet. Simultaneously, resulting from the practical limitations caused by experimental environment, each typical turbulence field has its own properties and imperfections as well, with the performance evaluations on their characteristic results have not been focused before. More studies need to be done on this subject consequently.

Though all these papers contribute greatly to the complicated correlations between turbulence flow and its impact factors, however, it can also be seen that their proposed impact mechanism models still hardly cover all involved participant elements ranged from experimental conditions to geometrical model properties. For the quantitatively discussion into their complicated mutual interaction principles still keeps a considerable distance from well-organized knowledge system, therefore those difficult unknown impacts mentioned before were still left in a state of un-studied or un-solved regrettably. As digital image ensures directly modeling of flow field, thereby a quantitatively assessment of the impact mechanism will improve the research quality in industry practice.

2. Partial Derivative Vectors

For statistics time points are $T=\{t_1,t_2,t_3,...t_n\}$, neighborhood coordinate space of block module $N_1\times N_2\times N_3$ is established in 3-D turbulence field. (Considering required precision of calculation and practical condition, we set the module's three-dimensional scale is $3\times3\times3$). The point (i,j,k) of module $f(x,y,z)$ is regarded as center, its 26 neighborhood's spatial coordinates are recoded, each velocity vector of marking point is showed in Eq. (1). Where $f(x,y,z)$ is centre point of module's space, $f(x-1,y-1,z+1)$, $f(x,y-1,z+1)$, $f(x-1,y+1,z+1)$, etc. are its neighborhoods, "→" labels the direction of spatial vector is from centre to neighborhood points, as showed in Fig. 1.

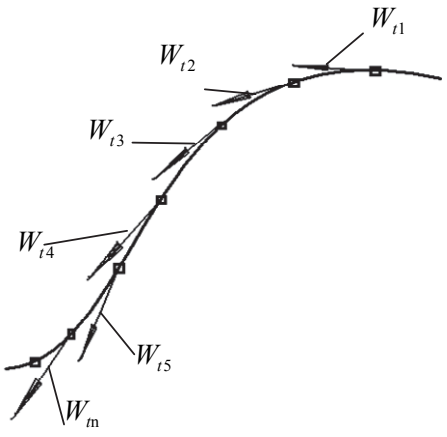

Fig. 1. Vectors of turbulence route.

Vectors can be calculated as:

$$\begin{cases}
\overrightarrow{\nabla_{-x,+y,+z}f(x,y,z)} = f(x,y,z) \rightarrow f(x-1,y+1,z+1)\\
\overrightarrow{\nabla_{x,+y,+z}f(x,y,z)} = f(x,y,z) \rightarrow f(x,y+1,z+1)\\
\overrightarrow{\nabla_{+x,+y,+z}f(x,y,z)} = f(x,y,z) \rightarrow f(x+1,y+1,z+1)\\
\overrightarrow{\nabla_{-x,y,+z}f(x,y,z)} = f(x,y,z) \rightarrow f(x-1,y,z+1)\\
\overrightarrow{\nabla_{x,y,+z}f(x,y,z)} = f(x,y,z) - \rightarrow f(x,y,z+1)\\
\overrightarrow{\nabla_{+x,y,+z}f(x,y,z)} = f(x,y,z) \rightarrow f(x+1,y,z+1)\\
\overrightarrow{\nabla_{-x,-y,+z}f(x,y,z)} = f(x,y,z) \rightarrow f(x-1,y-1,z+1)\\
\overrightarrow{\nabla_{x,-y,+z}f(x,y,z)} = f(x,y,z) \rightarrow f(x,y-1,z+1)\\
\overrightarrow{\nabla_{+x,-y,+z}f(x,y,z)} = f(x,y,z) \rightarrow f(x+1,y-1,z+1)
\end{cases}$$

$$\begin{cases}
\overrightarrow{\nabla_{-x,+y,z}f(x,y,z)} = f(x,y,z) \rightarrow f(x-1,y+1,z)\\
\overrightarrow{\nabla_{x,+y,z}f(x,y,z)} = f(x,y,z) \rightarrow f(x,y+1,z)\\
\overrightarrow{\nabla_{+x,+y,z}f(x,y,z)} = f(x,y,z) \rightarrow f(x+1,y+1,z)\\
\overrightarrow{\nabla_{-x,y,z}f(x,y,z)} = f(x,y,z) \rightarrow f(x-1,y,z)\\
\overrightarrow{\nabla_{+x,y,z}f(x,y,z)} = f(x,y,z) \rightarrow f(x+1,y,z)\\
\overrightarrow{\nabla_{-x,-y,z}f(x,y,z)} = f(x,y,z) \rightarrow f(x-1,y-1,z)\\
\overrightarrow{\nabla_{x,-y,z}f(x,y,z)} = f(x,y,z) \rightarrow f(x,y-1,z)\\
\overrightarrow{\nabla_{+x,-y,z}f(x,y,z)} = f(x,y,z) \rightarrow f(x+1,y-1,z)
\end{cases}$$

$$\begin{cases}
\overrightarrow{\nabla_{-x,+y,-z}f(x,y,z)} = f(x,y,z) \rightarrow f(x-1,y+1,z-1)\\
\overrightarrow{\nabla_{x,+y,-z}f(x,y,z)} = f(x,y,z) \rightarrow f(x,y+1,z-1)\\
\overrightarrow{\nabla_{+x,+y,-z}f(x,y,z)} = f(x,y,z) \rightarrow f(x+1,y+1,z-1)\\
\overrightarrow{\nabla_{-x,y,-z}f(x,y,z)} = f(x,y,z) \rightarrow f(x-1,y,z-1)\\
\overrightarrow{\nabla_{x,y,-z}f(x,y,z)} = f(x,y,z) \rightarrow f(x,y,z-1)\\
\overrightarrow{\nabla_{+x,y,-z}f(x,y,z)} = f(x,y,z) \rightarrow f(x+1,y,z-1)\\
\overrightarrow{\nabla_{-x,-y,-z}f(x,y,z)} = f(x,y,z) \rightarrow f(x-1,y-1,z-1)\\
\overrightarrow{\nabla_{x,-y,-z}f(x,y,z)} = f(x,y,z) \rightarrow f(x,y-1,z-1)\\
\overrightarrow{\nabla_{+x,-y,-z}f(x,y,z)} = f(x,y,z) \rightarrow f(x+1,y-1,z-1)
\end{cases} \quad (1)$$

Loading the record of time nodes, neighborhoods' motion vectors in different statistics time point are showed as: $\nabla f(t_1),\nabla f(t_2),\nabla f(t_3),..,\nabla f(t_n),t_i\in T$

The tangent vector of each point is:

$$\begin{cases}
W_{ut_1} = \nabla f(t_2) - \nabla f(t_1) = [p_{ut_1}, q_{ut_1}, r_{ut_1}]\\
W_{ut_2} = \nabla f(t_3) - \nabla f(t_2) = [p_{ut_2}, q_{ut_2}, r_{ut_2}]\\
\vdots\\
W_{ut_i} = \nabla f(t_{i+1}) - \nabla f(t_i) = [p_{ut_i}, q_{ut_i}, r_{ut_i}]
\end{cases} \quad (2)$$

W_{uuti} is the second-order partial derivative vector of specific curve's controlling point which represents variance ratio of tangent vector in the mathematical sense. After the tangent vectors are gotten, W_{uuti} can be calculated:

$$\begin{cases} W_{uut\,1} = [\,p_{uut\,1}, q_{uut\,1}, r_{uut\,1}\,] = W_{ut\,2} - W_{ut\,1} \\ \quad = [\,p_{ut\,2}, q_{ut\,2}, r_{ut\,2}\,] - [\,p_{ut\,1}, q_{ut\,1}, r_{ut\,1}\,] \\ W_{uu\,2} = [\,p_{uut\,2}, q_{uut\,2}, r_{uut\,2}\,] = W_{ut\,3} - W_{ut\,2} \\ \quad = [\,p_{ut\,3}, q_{ut\,3}, r_{ut\,3}\,] - [\,p_{ut\,2}, q_{ut\,2}, r_{ut\,2}\,] \\ \vdots \\ W_{uui} = [\,p_{uut\,i}, q_{uut\,i}, r_{uut\,i}\,] = W_{ut\,(i+1)} - W_{uti} \\ \quad = [\,p_{ut\,(i+1)}, q_{ut\,(i+1)}, r_{ut\,(i+1)}\,] - [\,p_{ut\,i}, q_{ut\,i}, r_{ut\,i}\,] \end{cases} \quad (3)$$

Turbulence route's tangent vector $W_{ti} = [p_{ut_i}, q_{ut_i}, r_{ut_i}]$ and second vector $W_{uui} = [p_{uut_i}, q_{uut_i}, r_{uut_i}]$ of each coordinate position are obtained [14].

3. Energy Optimization Fitting

Terzopoulos and Gossard have used laminose elastic deformation equation of elastic mechanics as their reference. Here we proposed model for free curve's establishment by energy optimization method [15]:

$$E_{curve} = \int (W_u^{\,2} + W_{uu}^{\,2} - 2w)du\,, \quad (4)$$

here W is curve which uses u as its parameter, W_u, W_{uu} are curve's first and second partial derivative vectors respectively.

In practical processing, the curve equation is transformed into form of B-spline function [16]:

$$w(u) = \sum_{i=0,m} V_i B_{i,s}(u)\,, \quad (5)$$

here V is controlling vertex of B-spline curve $w(u)$, $m+1$ is the number of controlling vertex, s is curve's power, and $B_{i,s}(u)$ is B-spline's primary function which is determined by power s and node vector $U=[u0, u1, u2,..., um+s+1]$.

For energy optimization curve fitting, we can obtain first derivatives $w_u(u)$ and second derivatives $w_u(u)$ from Eq. (5).

$$\begin{aligned} w_u(u) &= \sum_{i=0,m} V_i B'_{i,s}(u) \\ w_{uu}(u) &= \sum_{i=0,m} V_i B''_{i,s}(u) \end{aligned} \quad (6)$$

We substitute Eq. (6) into Eq. (5), and let f=0, through rearrangement that:

$$\begin{aligned} E &= \int_0^1 (\alpha \sum_{i=0,m}\sum_{j=0,m} V_i V_j B_{i,s}'(u) B_{j,s}'(u) + \\ &\quad \beta \sum_{j=0,m}\sum_{j=0,m} V_i V_j B_{i,s}''(u) B_{j,s}''(u))du \\ &= \alpha \sum_{i=0,m}\sum_{j=0,m} V_i V_j \int_0^1 B_{i,s}'(u) B_{j,s}'(u)\,du + \\ &\quad \beta \sum_{i=0,m}\sum_{j=0,m} V_i V_j \int_0^1 B_{i,s}'(u) B_{j,s}'(u)\,du \\ &= \sum_{i=0,m}\sum_{j=0,m} [V_i V_j * \int_0^1 (\alpha B_{i,s}'(u) B_{j,s}'(u) + \beta B_{i,s}''(u) B_{j,s}''(u))du] \end{aligned}$$

Then: $S_{i,j} = \int_0^1 (\alpha B_{i,s}'(u) B_{j,s}'(u) + \beta B_{i,s}''(u) B_{j,s}''(u))du$ (7)

Thus (4) can be simplified as:

$$E = \sum_{\substack{i=0,m \\ j=0,m}} (V_i * V_j \bullet S_{i,j})\,, \quad (8)$$

here $V_i * V_j$ represents the internal product of both sides. Under the condition of given definite number of s and KU, $S_{i,j}$ is integrating result of known function (constant number), thus energy model is transformed into a quadratic function labeled by the controlling vertex V [17].

4. Impact Mechanism

The basic thought of energy fairing is making surface's energy reach the minimum level under constraint condition. The surface fairing can be expressed by following optimization function [18]:

$$\begin{aligned} &\min E(V) \\ &D(v) = \sum_{i=1}^{n}\sum_{j=1}^{m} (V_{ij} \quad V_{ij}^{\,0})^2 < \varepsilon \end{aligned} \quad (9)$$

Here independent variable V is a vector constituted by surface's control vertexes. The objective function $E(V)$ reflects surface smoothness. If $E(V)$ lessen, surface is more smooth, and vice versa. The constraint condition $D(v)$ reflects the eccentricity between faired and original surfaces. ε is the given tolerance. If $D(v) < \varepsilon$, the eccentricity is in the permissible range. The definition expressions presented by *Kally* and *Ravani* are adopted for energy objective function [19]:

$$E(v) = \int (\alpha S_{uu}^{\,2} + \beta S_{uv}^{\,2} + \gamma S_{vv}^{\,2})dudv \quad (10)$$

Here α, β and γ are non-negative constant numbers, $S_{uu}^{\,2}, S_{uv}^{\,2}, S_{vv}^{\,2}$ are second- order derivative vectors of surface $S(u,v)$ in u,v directions. Thus:

$$\begin{aligned} E(V) = \int (&\alpha_{11} S_u^{\,2} + \alpha_{12}(S_u \times S_v)^2 + \alpha_{22} S_v^{\,2} + \beta_{11} S_{uu}^{\,2} \\ &+ \beta_{11} S_{uu}^{\,2} + \beta_{12} S_{uv}^{\,2} + \beta_{22} S)dudv \end{aligned} \quad (11)$$

If B-spline surface is defined as:

$$S_0(u,v) = \sum_{i=0}^{n}\sum_{j=0}^{m} B_{ip}(u)B_{jq}(v)V_{ij}^{\ 0}$$

$$S(u,v) = \sum_{i=0}^{n}\sum_{j=0}^{m} B_{ip}(u)B_{jq}(v)V_{ij}$$

$$\begin{aligned} S_{uu} &= \sum_{i=0}^{n}\sum_{j=0}^{m} B_{ip}(u)''B_{jq}(v)V_{ij} \\ S_{uv} &= \sum_{i=0}^{n}\sum_{j=0}^{m} B_{ip}(u)'B_{jq}(v)'V_{ij} \\ S_{vv} &= \sum_{i=0}^{n}\sum_{j=0}^{m} B_{ip}(u)B_{jq}(v)''V_{ij} \end{aligned}, \quad (12)$$

when we substitute Eq. (12) into energy objective function, then

$$E(V) = \sum_{i=0}^{n}\sum_{k=0}^{n}\sum_{j=0}^{m}\sum_{l=0}^{m}(V_{ij},V_{kl})C(i,j,k,l)$$

Here

$$\begin{aligned} C(i,j,k,l) = {} & \alpha\int B''_{ip}(u)B''_{kp}(u)du\int B_{jq}(v)B_{lq}(v)dv \\ & +\beta\int B'_{ip}(u)B'_{kp}(u)du\int B'_{jq}(v)B'_{lq}(v)dv \\ & +\gamma\int B_{ip}(u)B_{kp}(u)du\int B''_{jq}(v)B''_{lq}(v)dv \end{aligned} \quad (13)$$

For $A=(a_{ij})$, where $a_{(m+1)i+j,(m+1)k+l}=C(i,j,k,l)$, We set I is unit matrix and $B=A+VI$, $C=V$, when solving this equation, the controlling points of faired surface $S(u,v)$ can be obtained [20].

5. Experiment

Turbulence experiment and process analysis were started from an experiment of turbulence locus stipulation in the confined casing, Fig. 2 illustrates the experimental platform used for turbulence imaging and characteristic analyzing. Due to the process monitoring of turbulence experiment, a glass cylinder box was built up to simulate the confined space, with the CCD imaging system installed at the two peripheral outer-sides of this cylinder structure. Then the accurate image grabbing and turbulence motion locus detecting can be implemented by these imaging cameras through transparent glass wall. The three-dimensional size of this glass cylinder casing is *1 m×0.8 m ×0.6 m* with the depth of water-based enhanced fluid is 0.5 m.

One roller was auto-rotating at a high speed of 160 r/min, simultaneously it also revolving around its own central axis driven by the planetary gears at 50 r/min in the confined space. Impacted by centrifugal force and gravity force the water-base enhanced fluid is stirred and a high-speed turbulence be obtained, for the Reynolds number $\mathrm{Re}=uh/v$ in this experiment can be measured as 4700.

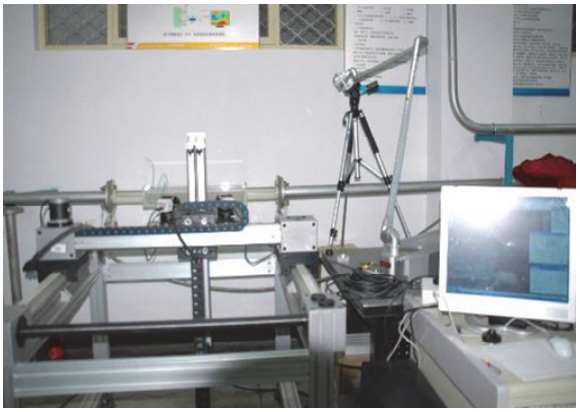

Fig. 2. The experimental platform used for turbulence imaging and characteristic analyzing.

DMIRM microscopic system manufactured by German LEICA was used to capture the three-dimensional motion locus information from this given turbulence flow field by digital micro-images, with the corresponding coordinate positions of these imaging CCD cameras were shown by the black circles, *M1, M2, M3* denote the amount of flow field grid points in the directions of *x, y, z* respectively. Combining with the practical experiment condition and precision requirement, the amount of grid points in three-dimensional direction was supposed as *100×80×60*.

In order to highlight the turbulence motion locus by tracer particles, these tracer particles were scattered into the turbulence flow field in an equally distribution, then their motion locus was traced and a series of sequential conjugate images was obtained. The black frame shows the moving process of these tracer particles. These digital images was set as the size of 4088×1288 with 256 gray level (0~255), and the development language of *Matlab7.0* was used to program the kernel analysis and computation module. Other experiment conditions are listed as follows: Celeron 2.26 microprocessor, 2G memory, operation system is Windows XP.

The motion locus of these tracer particles were measured and fitted in different flow velocities. In order to reflect the turbulence features, following common-used flow velocities are selected: *5 cm/s, 10 cm/s, 15 cm/s, 20 cm/s, 25 cm/s, 30 cm/s* and *35 cm/s*. Fig. 3 shows the key details of the fitted turbulence motion locus in three-dimensional coordinate system. Where the number value in X axis denotes the longitude coordinate position and the number value in Y axis denotes the traverse coordinate one in the horizontal plane, whose value scales ranged from -2 cm to 2 cm, on the other hand, the number value in Z denotes the vertical coordinate position with its value scale ranged from -4 cm to 4 cm. Based on this illustration can the spatial sketch of turbulence locus curves be clearly described. In this figure, the hollow dots denote the space coordinate positions of those tracer particles while real lines denote the fitted turbulence motion locus.

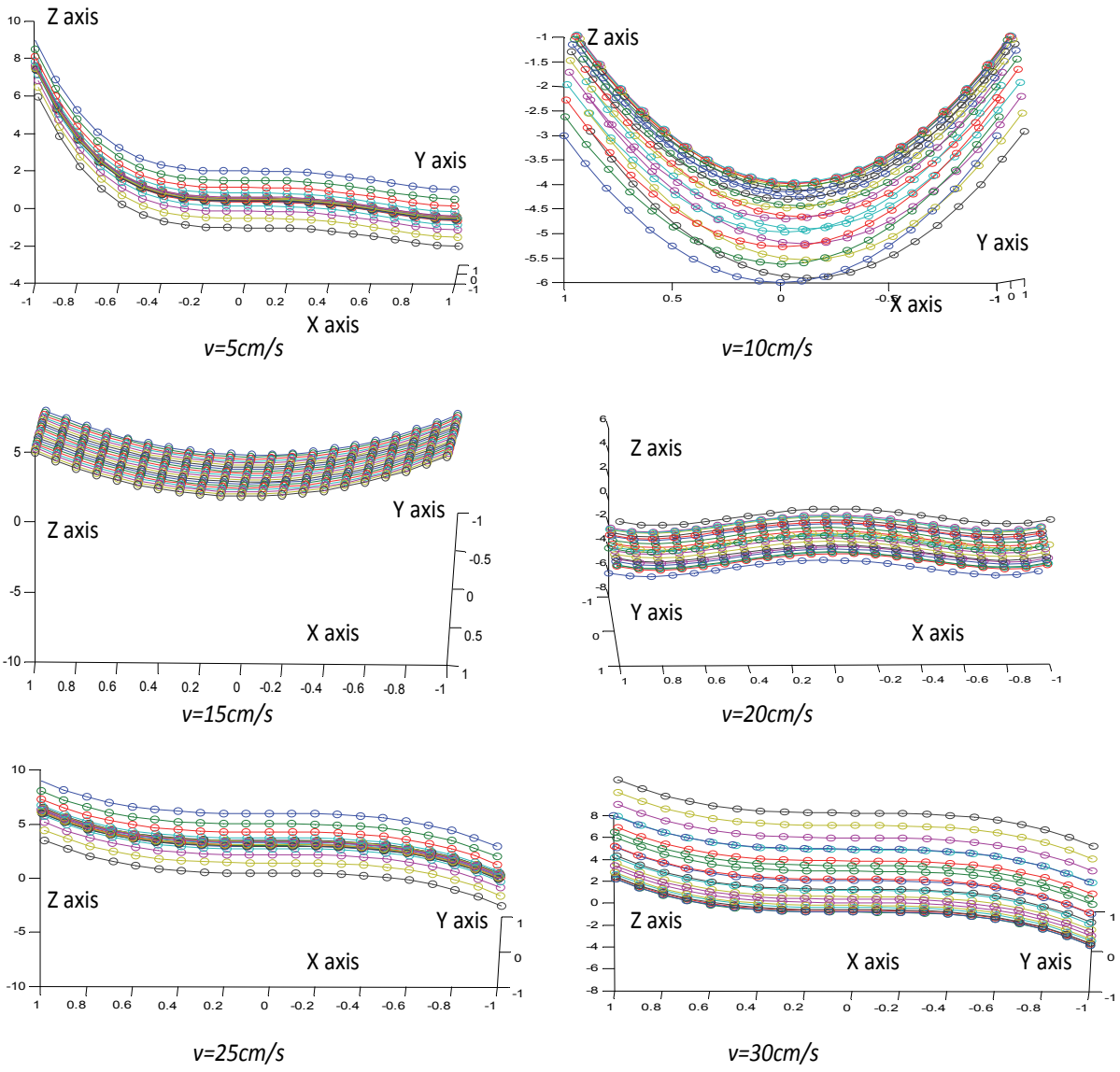

Fig. 3. Turbulence locus curves in three-dimensional coordinate system by using different flow velocities.

For index quantizing the image acquiring conditions, impact mechanisms exerting relative great impacts on image properties have been selected as follows: (1) light intensity, (2) exposing time, (3) light incident angle (the acute angle between light source's center-line and projecting vector-line on CCD imaging plane), (4) surface reflectivity of the tracing particle and (5) micro-magnification of turbulence image. All these selected parameters are adjusted meticulously around $\pm 3\% \sim \pm 10\%$ of the predetermined referential value. Based on a detailed comparison and data analysis, Table 1 describes the applied experimental conditions in different impact mechanisms for following turbulence research.

According to Eqs. (1~3) the sequence of evaluating parameters was established, then the image properties of different sub-images are computed, with the computed value results are demonstrated in Table 2. From this table a general sketch about the turbulence image features can be determined, including image energy, information entropy, inertia moment, image stability, image variance, distribute coefficient of image energy (EW), Zernike moment, signal-to-noise ratio of image (SNR), and signal-to-noise ratio of image. By using Eqs. (4~8) the relative weight values of fuzzy gray system are determined, then the fuzzy gray relational degrees between the impact mechanisms and the image properties were obtained by Eqs. (9~13), as shown by Table 3. In this table, the fuzzy gray relational degrees between following experimental conditions, including light intensity, exposing time for turbulence imaging, incident angle, surface reflectivity of tracer particles, imaging magnification, and those above-mentioned image properties were accurately calculated and clearly demonstrated, which contributes to the achievement of quantitatively comparison and process analysis for this experiment [20]. Thus the specific analysis and evaluation can be conducted.

Table 1. Conditions in different impact mechanisms.

	Light intensity	Exposing time	Incident angle	Surface reflectivity	Magnification
1	3450 lm	0.54 s	92.5°	0.8875	25
2	3360 lm	0.69 s	91.4°	0.8025	24
3	3010 lm	0.54 s	90.8°	0.8933	23
4	3000 lm	0.39 s	90.2°	0.8475	21
5	2980 lm	0.47 s	89.9°	0.9025	20
6	2800 lm	0.55 s	89.7°	0.9935	19
7	2590 lm	0.60 s	88.7°	0.9245	18
8	2400 lm	0.47 s	87.9°	0.9360	17
9	2300 lm	0.29 s	90.4°	0.8933	16
10	2100 lm	0.65 s	91.5°	0.8705	15

Table 2. Characteristic values of turbulence image samples.

Samples	Image energy	Information entropy	Inertia moment	Image stability	Image variance	EW	Zernike moment	SNR	Contrasting ratio
a	55.78	154.78	1485.6	885.6	1145.6	635.4	4578.9	0.639	0.587
b	48.99	115.63	1558.9	847.6	1826.5	785.5	4856.9	0.587	0.658
c	62.45	92.58	1702.6	802.6	1772.5	695.4	5587.9	0.802	0.782
d	53.69	158.77	1925.4	893.2	1635.5	802.4	5069.7	0.521	0.882
e	62.14	192.54	1847.5	702.5	1554.9	621.5	6021.1	0.589	0.698
f	70.25	165.48	1782.6	715.6	2014.6	458.6	6635.4	0.698	0.758
g	77.15	185.63	1695.4	772.5	1893.6	354.2	4926.5	0.889	0.902
h	65.89	202.54	1665.8	695.8	1478.5	446.2	4485.5	0.925	0.825
i	68.47	168.75	1477.8	648.2	1983.2	635.9	4756.8	0.921	0.887
j	69.22	188.92	1569.6	693.2	2006.5	664.2	8025.6	0.825	0.684

Table 3. Fuzzy gray relational degrees.

Impact factors	Image energy	Information entropy	Inertia moment	Image stability	Image variance	EW	Zernike moment	SNR	Contrasting ratio
Light intensity	0.785	0.847	0.563	0.902	0.665	0.554	0.485	0.695	0.665
Exposing time	0.856	0.925	0.801	0.936	0.814	0.602	0.554	0.665	0.475
Incident angle	0.514	0.921	0.874	0.845	0.725	0.702	0.725	0.458	0.485
Reflectivity	0.365	0.893	0.625	0.725	0.354	0.551	0.715	0.712	0.526
Magnification	0.335	0.702	0.502	0.901	0.601	0.635	0.624	0.225	0.428

6. Approximate Error

After fitting the turbulence curve's approximate error is analyzed. Let $f(t)(0 \le t \le 1)$ to be the B-spline curve which is defined by m controlling nodes and vectors $0=(\mu_0,\mu_1,..,\mu_{m-2},\mu_{m-1},\mu_m)=1$. Then one singles integral n is selected and be made $m \le 2^n+3$, thus we can approach curve $f(t)$ by the B-spline curve $f_n(t)$ which is defined by 2^n+3 controlling vertexes. U represents the congregation of all $f(t)$ node vectors, $U=\{\mu_0,\mu_1,..,\mu_{m-1},\mu_m\}$. Then approximate error of turbulence's curve is defined as:

$$\varepsilon_n = \max_{t \in U} |f(t) - f_n(t)| \tag{14}$$

PIV produced by US. TSI Co. is used for turbulence images' real time acquisition in different flow velocities. The PIV working frequency is 1500 Hz, laser wavelength is 530 nm, its image resolution is 1248×1024 pixels, and acquiring rate of digital images is 5 frm/s. In this experiment, we use fluorescent particle for monitoring turbulence, compare approximate error and curve's plane projection on three coordinate planes xoy, yoz, xoz by Eq. (9). The result is showed in Table 4 (unit: mm). The source and characteristic of approximate error are analyzed as follows: for turbulence's perturbation action is unavoidable, the route's tracing performance is worsen, thus fluid field's detail can't be displayed accurately, which leads the appearance of turbulence route's measuring error. On the other hand the existing mathematical truncating error also exerts negative influence

on fitting precision. But under current condition the approximate error gotten by new method still keeps at a relatively low level, which is within the traditional allowed range. When the flow velocity is increasing, the approximate error presents a tendency of steady decreasing.

Table 4. Fitting approximation error in different condition of flow velocity (mm).

Velocity	*xoy* plane	*yoz* plane	*xoz* plane
v=5 cm/s	0.78	1.26	1.09
v=10 cm/s	0.69	1.18	0.95
v=15 cm/s	0.45	0.99	0.88
v=20 cm/s	0.22	0.84	0.66
v=25 cm/s	0.20	0.63	0.59
v=30 cm/s	0.18	0.52	0.32

Comparing with other traditional research method, this method executes turbulence route's fitting and reconstructing directly. The fitted curve will facilities following research of turbulence discipline.

7. Impact Analysis

With the increment of light intensity, image luminance raises and its properties change. After comparing and analyzing, the fuzzy gray relational degrees between light intensity and such specific image properties as information entropy, image variance, signal-to-noise ratio, and contrasting ratio, are closely. Which means that intensity of light changes image's displaying properties, with light intensity is suggested in 2100 lm ~ 2600 lm.

Exposing time connects closely with those image properties such as information entropy, inertia moment, image stability and Zernike moment, etc. It was found that increasing exposing time facilitates the augment and stability of image information, and it is suggested that exposing time should be kept in 0.3 s~0.4 s.

By increasing incident angle of light, the luminance intensity per unit area of an image raises subsequently. As incident angle of light connects closely with image energy, inertia moment, image variance and contrasting ratio, etc. thus increasing incident angle facilitates a clear illustration of image properties, but it also raises the emerging probability of external interference as well, it is suggested that light incident angle should be kept in 89.5°~90.4°.

With the improvement of surface reflectivity on tracing particle, mirror reflection taking place gradually. This factor imposes a great impact on such properties as information entropy, image stability and contrasting ratio, etc. It is suggested that surface reflectivity of tracing particles should be kept in a relative low level, which facilitates the improvement of image quality and an accurate illustration of micro- topography of turbulence locus.

Micro-magnification keeps a close fuzzy gray relationship with information entropy, inertia moment, signal-to-noise ratio, etc. With a clear displaying of turbulence micro-properties, micro-magnification is impacted seriously by the turbulence locus topography. Over-magnification debases image quality, thus it is suggested that magnification factor in this experiment be kept in 22~26.

8. Conclusions

The impact mechanisms of the turbulence image properties were assessed by using fuzzy gray theory. Through calculating the gray relational degrees between those selected impact mechanisms and turbulence image properties, their influential tendency can be analyzed and its variance discipline was quantified. This study solves the difficulties of quantitative assessing the impact mechanisms of turbulence images in a traditional analysis. As the experimental process has a deliberate theoretical foundation thus the mathematical analyzing process can be simplified; finally a series of experimental suggestions and new ideas for following turbulence research were also presented as well.

Acknowledgements

The author acknowledges the funding of following science foundation: National Natural Science Foundation of China (No. 51205073), China Postdoctoral Science Foundation funded project (No. 2013T60797, No. 2012M510197), the Irrigation Science and Technology Research Project of Guangdong Province (No. 2012-11), the Project of Department of Education of Guangdong Province (No. 2013KJCX0142), the Science and Technology project of Guangzhou city (No. 2012J4100053, 12C42011566), the Research Project of Guangzhou Municipal University (No. 10A068), the Foundation Project of The State Key Laboratory of Fluid Power Transmission and Control, Zhejiang University (No. GZKF-201201); the Foundation Project of Traction Power State Key Laboratory, Southwest Jiaotong University (No.TPL1311) and the Foundation Project of the National Engineering Research Centre of Near-Net-Shape Forming for Metallic Materials, South China University of Technology (No. 2012007) are also appreciated for supporting this work. We also want to thank the editors for their hard work and the referees for their comments and valuable suggestions to improve this paper.

References

[1]. Thrasyvoulos Panidis, Demosthenes D. Papailiou, The structure of two-phase grid turbulence in a rectangular channel: an experimental study, *International Journal of Multiphase Flow*, 26, 8, 2000, pp. 1369-1400.

[2]. Serhat Kucukali, Hubert Chanson, Turbulence measurements in the bubbly flow region of hydraulic jumps, *Experimental Thermal and Fluid Science,* 33, 1, 2008, pp. 41-53.
[3]. Satya P. Ojha, B. S. Mazumder, Turbulence properties of flow region over a series of 2-D dune shaped structures, *Advances in Water Resources*, 31, 3, 2008, pp. 561-576.
[4]. John Villasenor, Alain Vincent, An algorithm for space recognition and time tracking of vortices tubes in turbulence, *Image Understanding*, 55, 1, 1992, pp. 27-35.
[5]. Xinhong Liu, Yuyun Bao, Zhipeng Li, Zhengming Gao, John M. Smith, Particle Image Velocimetry Study of Turbulence Properties in a Vessel Agitated by a Dual Rushton Impeller, *Chinese Journal of Chemical Engineering*, 16, 5, 2008, pp. 700-708.
[6]. L. Nikiforaki, G. Montante, K. C. Lee, M. Yianneskis, On the origin, frequency and magnitude of macro-instabilities of the flows in stirred vessels, *Chemical Engineering Science*, 58, 13, 2003, pp. 2937-2949.
[7]. Manabendra Pathak, Anupam Dewan, Anoop K. Dass, An assessment of streamline curvature effects on the mixing region of a turbulent plane jet in cross-flow, *Applied Mathematical Modelling*, 29, 8, 2005, pp. 711-725.
[8]. Sagar S. Deshpande, Jyeshtharaj B. Joshi, V. Ravi Kumar, B. D. Kulkarni, Identification and characterization of flow structures in chemical process equipment using multi-resolution techniques, *Chemical Engineering Science*, 63, 21, 2008, pp. 5330-5346.
[9]. Gwang Hoon Rhee, Hyung Jin Sung, Numerical prediction of locally forced turbulent separated and reattaching flow, *Fluid Dynamics Research*, 26, 6, 2000, pp. 421-436.
[10]. A. S. Pereira, F. T. Pinho, Re-circulating turbulent flows of thixotropic fluids, *Journal of Non-Newtonian Fluid Mechanics,* 99, 2-3, 2001, pp. 183-201.
[11]. Bruce L. Rhoads, Stephen T. Kenworthy, Flow structure at an asymmetrical stream confluence, *Geomorphology*, 11, 4, 1995, pp. 273-293.
[12]. Wang Zhen-Bo, Ma Yi, Jin You-Hai, Simulation and experiment of flow field in axial-flow hydro-cyclone, *Chemical Engineering Research and Design*, 89, 6, 2011, pp. 603-610.
[13]. E. A. Luke, P. Cinnella, Numerical simulations of mixtures of fluids using upwind algorithms, *Computers & Fluids*, 36, 10, 2007, pp. 1547-1566.
[14]. Ding-An Chiang, Louis R. Chow, Nan-Chen Hsien, Fuzzy information in extended fuzzy relational databases, *Fuzzy Sets and Systems*, 92, 10, 1997. pp. 1-20.
[15]. Xiaohui Tang, Guoqing Chen, Equivalence and transformation of extended algebraic operators in fuzzy relational databases, *Fuzzy Sets and Systems*, 157, 20, 2006, pp. 1581-1596.
[16]. C. M. B. Nobre, R. A. Braga Jr, A. G. Costa, R. R. Cardoso, W. S. da Silva, T. Sáfadi, Bio-speckle. Laser spectral analysis under Inertia Moment, Entropy and Cross-Spectrum methods, *Optics Communications*, 282, 1, 2009, pp. 2236-2242.
[17]. Deniz Erdogmus, Erik G. Larsson, Rui Yan, Jose C. Principe, Jeffrey R. Fitzsimmons, Measuring the signal-to-noise ratio in magnetic resonance imaging: a caveat, *Signal Processing,* 84, 10, 2004, pp. 1035-1040.
[18]. Jingyu Hua, Limin Meng, Zhijiang Xu, Gang Li, An adaptive signal-to-noise ratio estimator in mobile communication channels, *Digital Signal Processing*, 20, 12, 2010, pp. 692-698.
[19]. Y. Z. Chen, Complex potentials and singular integral equation for curve crack problem in antiplane elasticity, *International Journal of Engineering Science*, 38, 3, 2000, pp. 565-574.
[20]. Michael Griebel, Gerhard Zumbusch, Parallel adaptive subspace correction schemes with applications to elasticity, *Computer Methods in Applied Mechanics and Engineering*, 184, 10, 2000, pp. 303-332.